ADVANCED MATERIALS INTERFACES
Open Access
www.advmatinterfaces.de

Check for updates

Rear Interface Engineering in Solution-Processed Submicron $Cu(In,Ga)(S,Se)_2$ Solar Cells on Transparent $Sn:In_2O_3$ Back Contact

Yao Gao, Guanchao Yin, and Martina Schmid**

The parasitic absorption in $Cu(In,Ga)(S,Se)_2$ (CIGSSe) solar cells emerging from the Mo back contact can be significantly reduced by replacing it with tin-doped indium oxide (ITO). Commonly, an undesirable GaO_x layer forms at the CIGSSe/ITO interface during the high-temperature fabrication process, which has a detrimental effect on photo-carrier extraction. Here, a Cu-In-TU-DMF (TU: thiourea, DMF: N, N-Dimethylformamide) intermediate layer for modification of the CIGSSe/ITO interface, which improves the efficiency of submicron CIGSSe solar cells significantly, is reported about. The reference submicron CIGSSe solar cells exhibit inferior performance (2.4% efficiency) and a large open circuit voltage deficit ($V_{oc,def}$ = 815.9 mV) due to a high barrier at the CIGSSe/ITO interface. At the modified rear interface, the recombination is reduced and hence carrier transport and collection are obviously improved. The efficiency of submicron CIGSSe solar cells on ITO with rear interface modification achieves 7.9% with an open circuit voltage of 565.8 mV, a short circuit current density of 23.4 mA cm^{-2}, and a fill factor of 59.5%, as well as a $V_{oc,def}$ of 589.2 mV.

1. Introduction

The champion efficiency of copper indium gallium disulfoselenide [$Cu(In,Ga)(S,Se)_2$: CIGSSe] thin film solar cells has achieved 23.6%, which makes them a promising alternative to silicon solar cells.[1] The best-performing CIGSSe solar cells are deposited by vacuum methods, which are expensive techniques due to complex fabrication conditions.[2] In contrast, solution-processed CIGSSe thin film fabrication presents the potential for cost-effectiveness and high throughput.[3] The molecular precursor solution approach has many advantages, such as simple solution preparation, high material utilization rate, adaptability to roll-to-roll processing, precise control of element composition, and large-area homogeneity.[2a,3e,f,4] However, the optimal performance of solution-processed CIGSSe solar cells is achieved from a hydrazine-based precursor solution, which prohibits its industrial production for health, environment, and safety concerns.[3c] Jiang et al. have proven that efficiencies of 14.5% for $CuIn(S,Se)_2$ (CISSe) and 15.2% for $Cu(In,Ga)(S,Se)_2$ (CIGSSe) solar cells can be obtained from a metal-chloride-TU-DMF (TU: thiourea, DMF: N, N-Dimethylformamide) precursor solution, which offers an alternative path to replace the highly toxic hydrazine precursor process.[4b] Furthermore, a reduction of material consumption along with a shortening of the deposition duration can be achieved by thinning the absorber thickness to submicron (absorber thickness < 1 µm). In addition, a submicron CIGSSe absorber can reduce the pathway for electron/hole extraction and improve the homogeneity of the absorber and therefore is promising for cost-effective and efficient solar cells.[5]

Typically, molybdenum (Mo) is used as a back contact material for various chalcogenide thin film solar cells due to the formation of the favorable quasi-Ohmic contact at the absorber/Mo interface. However, the Mo back contact has strong parasitic absorption, leading to an increase in optical losses for submicron cells.[6] Compared to the opaque Mo back contact, the fabrication of CIGSSe absorbers on transparent conductive oxide (TCO) back contacts can reduce the optical losses of the solar cells and open up further application areas.[2b,7] Various TCOs, such as tin-doped indium oxide (ITO), fluorine-doped tin oxide (FTO), and aluminum-doped zinc oxide (AZO), have been used as back contact of CIGSSe solar cells.[3a,8] However, the highly resistive GaO_x layer forming at the CIGSSe/TCO rear interface during the high-temperature CIGSSe growth (temperatures above 520 °C) leads to blocking the hole extraction from the CIGSSe absorber.[3a,8c]

Y. Gao, M. Schmid
Department of Physics and Center for Nanointegration Duisburg-Essen (CENIDE)
University of Duisburg Essen
Forsthausweg 2, 47057 Duisburg, Germany
E-mail: martina.schmid@uni-due.de
G. Yin
School of Materials Science and Engineering
Wuhan University of Technology
Luoshi Road 122, Wuhan 430070, China
E-mail: guanchao.yin@whut.edu.cn

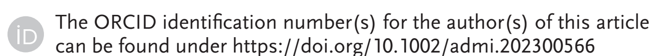
The ORCID identification number(s) for the author(s) of this article can be found under https://doi.org/10.1002/admi.202300566

© 2023 The Authors. Advanced Materials Interfaces published by Wiley-VCH GmbH. This is an open access article under the terms of the Creative Commons Attribution License, which permits use, distribution and reproduction in any medium, provided the original work is properly cited.

DOI: 10.1002/admi.202300566

© 2023 The Authors. Advanced Materials Interfaces published by Wiley-VCH GmbH

21967350, 0, Downloaded from https://onlinelibrary.wiley.com/doi/10.1002/admi.202300566 by Universitaet Duisburg-Essen, Wiley Online Library on [07/11/2023]. See the Terms and Conditions (https://onlinelibrary.wiley.com/terms-and-conditions) on Wiley Online Library for rules of use; OA articles are governed by the applicable Creative Commons License

Figure 1. The recipe of CIGSSe absorbers with or without interface treatment.

Therefore, the rear interface composition plays a crucial role in obtaining high-efficient CIGSSe solar cells on TCO.

So far, the maximum efficiency achieved for solution-processed CIGSSe on TCO back contacts is only 6%.[3a] High-quality CIGSSe solar cells on TCO can be fabricated at low substrate temperature by a co-evaporation process.[6b,d] However, when the solution-processed precursor films are selenized at low temperatures, the rear side of the absorber consists of an undesirable fine-grained layer, which can be related to high recombination.[8a] Therefore, there are still enormous challenges in fabricating high-quality CIGSSe on TCO back contacts by solution processing. Inserting a thin Mo layer between the CIGSSe and TCO back contact is a potential strategy to overcome this challenge because it allows CIGSSe absorber growth at high temperatures without the formation of GaO_x.[2d,8c,9] However, the parasitic optical absorption of Mo is a challenge in improving the usage of unabsorbed light supposed to be, e.g., reflected back into the absorber by a reflective mirror from the back side of the glass.[2b,c,e,6c] In our previous research, an 8% efficient CISSe (no Ga) solar cell with a submicron absorber has been successfully fabricated on ITO back contact by selenizing the solution-processed metal-chloride-DMF precursor film at 520 °C.[10] However, open-circuit voltage (V_{oc}) and fill factor (*FF*) are still low, which limits further efficiency improvement. Therefore, CIGSSe solar cells including gallium are favorable due to the expected higher V_{oc} and efficiency compared to CISSe owing to the widened bandgap with increasing Ga content.[4b] Given the achieved good performance of CISSe on ITO, introducing a thin electrically beneficial CISSe layer at the CIGSSe/ITO interface is a potential strategy for achieving high-efficiency CIGSSe solar cells fabricated via the solution process.

In this work, we report on cost-efficient CIGSSe solar cells deposited from metal-chloride-DMF solution on ITO back contact. A thin Cu-In-TU-DMF layer is pre-deposited on the ITO back contact for interface modification before the Cu-In-Ga-TU-DMF precursor solution. This modification layer is applied to reduce the Ga concentration at the rear interface of the CIGSSe absorber. The lower Ga concentration favors obtaining a high-quality CIGSSe absorber and hinders the formation of the GaO_x interlayer. The modified interface reduces the back barrier height and significantly improves the photovoltaic (PV) performance. We demonstrate a power conversion efficiency (*PCE*) of 7.9% for this CIGSSe solar cell with a thin Cu-In-TU-DMF interface modification layer.

2. Results

Figure 1 shows the schematic illustration of the structure without/with a Ga-free modification layer (Cu-In-TU-DMF). In brief, the Ga-free layer is firstly spin-coated on ITO back contact.

The elemental distributions of the absorbers are measured by GD-OES and are presented in **Figure 2** and Figure S1 (Supporting Information). Both reference CIGSSe (R-CIGSSe) and interface modification treatment CIGSSe (T-CIGSSe) show lower Na concentrations near the front surface than in the absorber bulk (Figure 2a). The R-CIGSSe absorber presents a significantly higher Na concentration in the bulk of the absorber (from 15% depth toward the rear surface) than the T-CIGSSe absorber. However, a reverse trend is observed near the front surface (0–15% depth). The T-CIGSSe absorber displays a mostly uniform and low concentration of Na, which can be attributed to a small amount of Na diffusing into the T-CIGSSe absorber from the SLG substrate. In the solution process, high-quality and dense chalcopyrite absorbers grow from the liquid-phase $Cu_{2-x}Se$ compound.[4b] Compared to the lattice constant of $CuGaSe_2$ (0.560 nm), $CuInSe_2$ (0.578 nm) and $Cu_{2-x}Se$ (0.579 nm) have highly similar lattice constants, resulting in the formation of a dense layer on the bottom of the T-CIGSSe absorber.[11] From this, it is concluded that the T-CIGSSe absorber receives a lower Na concentration than the R-CIGSSe absorber. A high Na content will promote GaO_x formation during the absorber growth at a high temperature.[12] Therefore, this thin In-rich interface modification layer favors the formation of a dense benign electrical rear interface, which can reduce the diffusion of Na, resulting in hindering the GaO_x formation. As can be seen in Figure 2b, the Cu/(Ga+In) (CGI) ratio in R-CIGSSe and T-CIGSSe absorbers increases toward the front surface, yet drops in its direct vicinity. The T-CIGSSe absorber shows a wider Cu-depletion at the front surface compared to the R-CIGSSe absorber. Na can occupy Cu vacancies (Na_{Cu}) of the CIGSSe absorber, leading to a low Cu concentration in the bulk of the R-CIGSSe absorber (15–70% absorber depth) with a relatively high Na concentration.[4b,13] Both of these two CIGSSe absorbers exhibit a similar tendency of Ga/(In+Ga) ratio (GGI) (Figure 2c), which can be attributed to the inter-diffusion of In and Ga. Ga diffuses toward the rear side and In migrates toward the front side of the absorber.[2a,6a,8c,11] The maximum GGI occurs at a depth of ≈70%. Simultaneously, an overall larger GGI exists in the R-CIGSSe absorber than in the T-CIGSSe absorber due to the lack of a Ga-free modification layer in R-CIGSSe (Figure 1). A pronounced

© 2023 The Authors. Advanced Materials Interfaces published by Wiley-VCH GmbH

21967350, 0, Downloaded from https://onlinelibrary.wiley.com/doi/10.1002/admi.202300566 by Universitaet Duisburg-Essen, Wiley Online Library on [07/11/2023]. See the Terms and Conditions (https://onlinelibrary.wiley.com/terms-and-conditions) on Wiley Online Library for rules of use; OA articles are governed by the applicable Creative Commons License

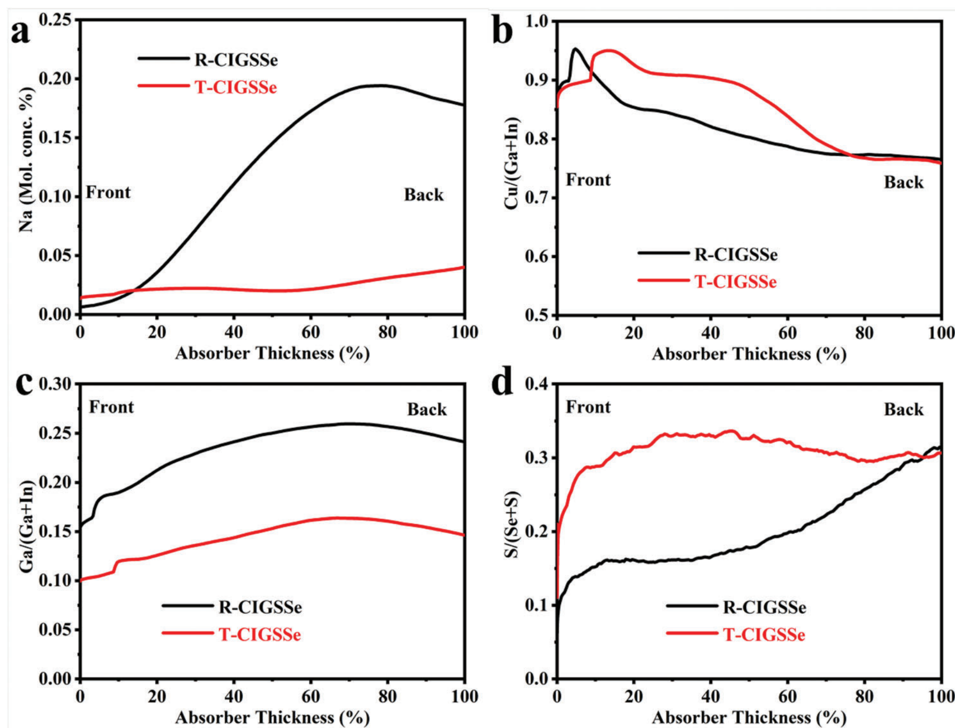

Figure 2. a) Na concentration profiles, b) Cu/(Ga+In), c) Ga/(Ga+In), and d) S/(Se+S) ratios of absorbers measured by GDOES. The *x*-axis is normalized to 100% absorber thickness.

increase in the S/(Se+S) ratio toward the rear interface is observed in the R-CIGSSe absorber in contrast to a high and homogeneous distribution for T-CIGSSe (Figure 2d). It is reported that In_2S_3 shows a lower standard molar formation enthalpy (−427.0 kJ mol^{-1}) at 298.15 K than In_2Se_3 (−78 kJ mol^{-1}), indicating that In_2S_3 forms easier than In_2Se_3. T-CIGSSe presents a higher CGI than R-CIGSSe in the 15–70% absorber depth (Figure 2b), which can benefit large grain formation and reduce the grain boundaries.[14] However, the volatilization of elemental S is along the grain boundaries. The formation of In_2S_3 and reduction of grain boundaries hinder the volatilization of elemental S in the T-CIGSSe (S comes from the thiourea of the precursor solution), leading to the high concentration of S in the T-CIGSSe absorber.

Cross-sectional SEM images of the CIGSSe devices are shown in **Figure 3**. The thicknesses of the CIGSSe absorbers are 730 nm. The R-CIGSSe absorber can be divided into an ≈ 300 nm thick layer with small grains on top and a 400 nm thick layer with a non-uniform size of CIGSSe grains on the bottom (Figure 3a). Larger grains on the bottom can be attributed to the high content of Na (Figure 2a). Unlike the R-CIGSSe absorber, a large-grained top layer of ≈450 nm is observed in the T-CIGSSe absorber (Figure 3b), which can be explained by a slightly higher Na content near the front surface (0–15% depth of absorber) of the T-CIGSSe. A continuous dense bottom layer is observed in the T-CIGSSe. It has been proven that CISe and $Cu_{2-x}Se$ have a similar lattice constant, and the CISe absorber is denser than the CGSe absorber.[10] When the absorbers have similar Cu

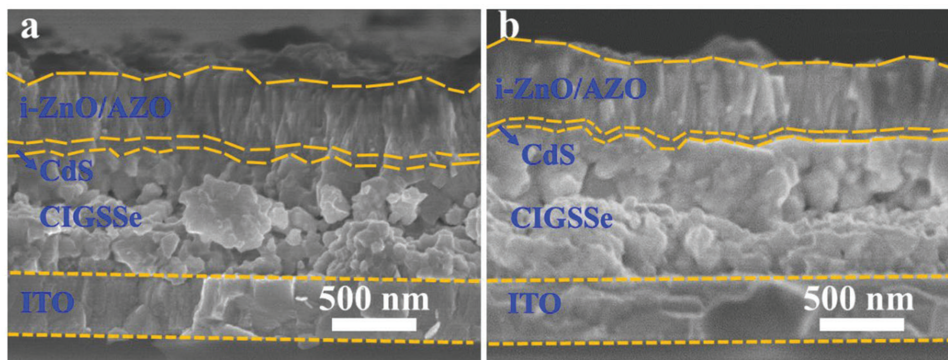

Figure 3. Cross-sectional SEM images of the a) R-CIGSSe and b) T-CIGSSe device.

 © 2023 The Authors. Advanced Materials Interfaces published by Wiley-VCH GmbH

21967350, 0, Downloaded from https://onlinelibrary.wiley.com/doi/10.1002/admi.202300566 by Universitaet Duisburg-Essen, Wiley Online Library on [07/11/2023]. See the Terms and Conditions (https://onlinelibrary.wiley.com/terms-and-conditions) on Wiley Online Library for rules of use; OA articles are governed by the applicable Creative Commons License

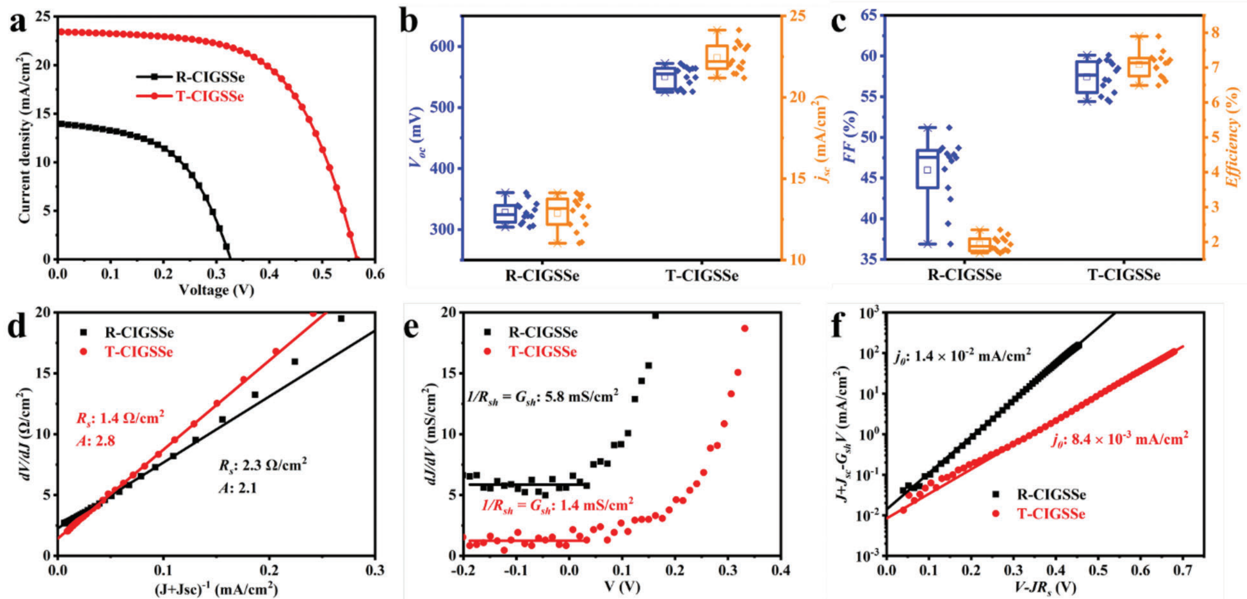

Figure 4. a) J–V curves of the best CIGSSe solar cells; b) statistical distributions of open circuit voltage V_{oc}, short current density j_{sc}, c) fill factor FF and efficiency derived from 14 devices for each fabrication method; d) dV/dJ as a function of $1/(J + J_{sc})$ with a linear fit to extract R_s from the y-intercept and A from slope, e) dV/dJ versus V for R_{sh} extraction, f) $\ln(J+J_{sc}-G_{sh}V)$ versus $V-JR_s$ with fit to determine j_0. (d–f) refer to the best CIGSSe solar cells.

content, the In-rich absorber consists of uniform and dense grains rather than the Ga-rich absorber.[11] As both absorbers show similar CGI ratios in 75–100% depth (Figure 2b), the dense bottom layer of the T-CIGSSe absorber consisting of uniform grains is ascribed to the smaller GGI (Figure 2c).

Figure 4a presents the current density-voltage (J–V) curves of the best R-CIGSSe and T-CIGSSe devices. A power conversion efficiency (PCE) of 2.4% is obtained for the R-CIGSSe solar cell with V_{oc} = 327.1 mV, j_{sc} = 14.0 mA cm^{-2}, and FF = 51.2%. When a Cu-In-TU-DMF layer is applied for rear interface modification, the PCE of the resulting T-CIGSSe device is significantly improved to 7.9% with V_{oc} = 565.8 mV, j_{sc} = 23.4 mA cm^{-2}, and FF = 59.5%. The improvement of PCE of the T-CIGSSe device can be ascribed to the remarkable increase in V_{oc} and j_{sc}. The statistical distributions of the photovoltaic parameters for 14 CIGSSe sub-cells of each recipe are shown in Figure 4b,c. PCE, V_{oc}, j_{sc}, and FF of the T-CIGSSe devices are superior to those of the R-CIGSSe devices, implying that the rear interface modification is an effective strategy to obtain high-efficiency CIGSSe solar cells on TCO.

The series resistance (R_s), the shunt conductance (G_{sh}), the shunt resistance (R_{sh}), the ideality factor (A), and the reverse saturation current density (j_0) are calculated from the illuminated J–V curves by applying the Hegedus method to the equation[2b,10,15]:

$$j(V) = j_0 \exp\left[\frac{q}{AkT}\left(V - jR_s\right)\right] + G_{sh}V - j_{sc} \quad (1)$$

where q is the elementary charge and k the Boltzmann constant. The resulting electrical parameters are presented in Figure 4 and are summarized in **Table 1**. The best T-CIGSSe device exhibits a smaller R_s and a larger R_{sh}, indicating that the Cu-In-TU-DMF interface modification can improve the charge transport and reduce the recombination (bulk and interface recombination) (Figure 4d,e).[2d,8c] The smaller j_0 in the T-CIGSSe device confirms reduced bulk recombination (Figure 4f). Therefore, the T-CIGSSe device presents better PV performance. However, the ideality factor is higher with interface modification (Figure 4d and Table 1), which can be explained by the high Na content near the front surface of the T-CIGSSe absorber (Figure 2).[16] This high Na-content will occupy the Cu vacancies and form Na_{Cu} defects, which will hinder the Cd^{2+} diffusion and formation of Cd_{Cu} donor defects during the CdS chemical bath deposition process. Yet, the PV performance of T-CIGSSe solar cells is still superior to one of the R-CIGSSe devices, indicating that the front surface is not the main reason for limiting the efficiency of CIGSSe solar cells.

EQE measurements of the respectively best R-CIGSSe and T-CIGSSe devices are depicted in **Figure 5**a. They show a similar EQE in the short wavelength range (300–390 nm). Yet, the T-CIGSSe device exhibits a significantly higher spectral response from 390 to 1100 nm wavelength. The bandgap (E_g) values of the two cells are obtained from the plot of $[E\times\ln(1\text{-EQE})]^2$ versus E.[10] The E_g of R-CIGSSe is 1.143 eV, while it is 1.155 eV for T-CIGSSe (inset in Figure 5a). The slight increase in E_g by

Table 1. Photovoltaic parameters of the best CIGSSe device with or without interface modification.

	PCE [%]	V_{oc} [mV]	j_{sc} [mA cm^{-2}]	FF [%]	R_s [Ω cm^2]	G_{sh} [mS cm^{-2}]	R_{sh} [Ω cm^2]	A	j_0 [mA cm^{-2}]
R-CIGSSe	2.4	327.1	14.0	51.2	2.3	5.8	178.1	2.1	1.4×10^{-2}
T-CIGSSe	7.9	565.8	23.4	59.5	1.4	1.4	714.3	2.8	8.4×10^{-3}

© 2023 The Authors. Advanced Materials Interfaces published by Wiley-VCH GmbH

21967350, 0, Downloaded from https://onlinelibrary.wiley.com/doi/10.1002/admi.202300566 by Universitaet Duisburg-Essen, Wiley Online Library on [07/11/2023]. See the Terms and Conditions (https://onlinelibrary.wiley.com/terms-and-conditions) on Wiley Online Library for rules of use; OA articles are governed by the applicable Creative Commons License

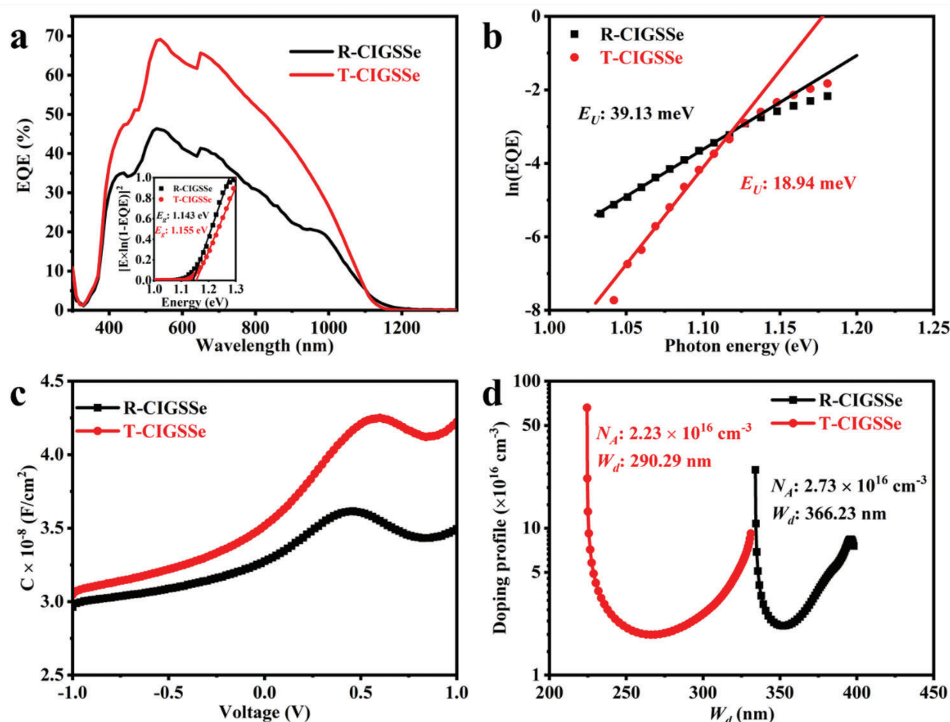

Figure 5. a) External quantum efficiency, inset: bandgap extraction, b) ln(EQE) as a function of photon energy at the long-wavelength edge to determine the Urbach energy E_U, c) C–V curves, and d) doping profiles for the best R-CIGSSe and T-CIGSSe solar cell.

0.012 eV can be ascribed to the higher S content of the T-CIGSSe absorber (Figure 2d). The Urbach energy (E_U) can be extracted from the EQE at the long-wavelength edge and reflects the carrier mobility and lifetime of the solar cells.[16] Figure 5b shows the according relation between ln(EQE) and photon energy: E_U = 39.13 meV is obtained for the R-CIGSSe solar cell and reduces to 18.94 meV for T-CIGSSe, implying a significantly improved absorber quality.[16] The deficit in open circuit voltage, $V_{oc,def}$, calculated as the difference of this bandgap value (divided by the elementary charge) and the open circuit voltage from Table 1, is given in **Table 2**. It reduces from 815.9 to 589.2 mV, i.e., by > 25% relative, with interface modification, and can partially be explained by a smaller E_U value of the T-CIGSSe device.[16a]

Figure 5d shows the acceptor doping density (N_A) and the width of the depletion region (W_d) of the highest efficient CIGSSe solar cells of each type extracted from the room temperature C–V profiles (Figure 5c). The R-CIGSSe device exhibits a larger N_A and a wider W_d than the T-CIGSSe one (Figure 5d and Table 2), which may originate from the high Na content in the bulk and the low Na content near the front surface of the R-CIGSSe absorber (Figure 2a), leading to increased charge carrier concentration and improved pn-junction formation, respectively. Generally, a wide W_d can promote the separation of photo-generated electron-hole pairs and benefit carrier transportation.[17] However, the PV performance of the R-CIGSSe device is significantly inferior. Therefore, the limitation of high-efficiency achievement in R-CIGSSe may come from the CIGSSe/ITO interface.

Figure 6 shows the temperature versus voltage plot obtained from temperature-dependent current density-voltage measurements of the CIGSSe solar cells. The activation energy E_a can be extracted from the $JV(T)$ profiles by linear extrapolation of V_{oc} to $T = 0$ K according to the equation[2b,6b]:

$$V_{oc} = \frac{E_a}{q} - \frac{AkT}{q} \ln\left(\frac{j_{00}}{j_{sc}}\right) \quad (2)$$

where j_{00} denotes the prefactor of saturation current density. Generally, when CIGSSe absorbers are fabricated on Mo back contact, E_a is close to E_g owing to a quasi-Ohmic contact assisted by the formation of $Mo(S,Se)_2$. However, there is a non-negligible back barrier (Φ_B) remaining at the CIGSSe/ITO interface. The sheet resistance of the as-sputtered ITO back contact is 32.02 Ω sq^{-1} and it can reduce to 17.14 Ω sq^{-1} after being subjected to pre-annealing at 500 °C for 10 min (Figure S2, Supporting Information). The sheet resistance of the ITO back contact in the completed CIGSSe solar cells further reduces to 9.15 Ω sq^{-1}, which is

Table 2. Optoelectronic device properties of the best R-CIGSSe and the best T-CIGSSe solar cells.

	E_g [eV]	E_U [meV]	N_A [cm^{-3}]	W_d [nm]	E_a [eV]	$V_{oc,def}$ [mV]	Φ_B [eV]
R-CIGSSe	1.143	39.13	2.73×10^{16}	366.23	0.644	815.9	0.499
T-CIGSSe	1.155	18.94	2.23×10^{16}	290.29	1.116	589.2	0.039

© 2023 The Authors. Advanced Materials Interfaces published by Wiley-VCH GmbH

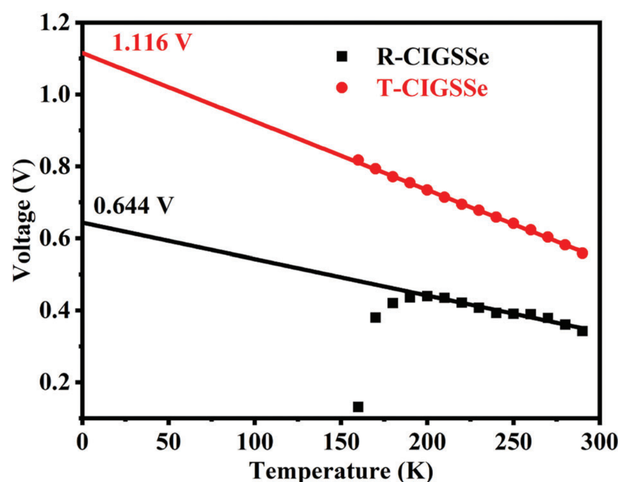

Figure 6. Temperature-dependent open-circuit voltage of CIGSSe solar cells and linear extrapolations to $T = 0$ K.

measured by mechanically removing the CIGSSe absorber. However, this sheet resistance is still higher than the 0.3 Ω sq^{-1} for Mo after CIGSSe removal. Therefore, E_g-Φ_B should be considered in Equation (2) rather than E_a, and the back barrier height can be extracted as $\Phi_B = E_g$-E_a.[2b,6b]

A small value of $E_a = 0.644$ eV is observed for the R-CIGSSe device, revealing a large gap compared with E_g and thus pointing to interface recombination (Figure 6 and Table 2).[6b,18] There are two interfaces in the CIGSSe absorber: the CdS/CIGSSe front interface and the CIGSSe/ITO rear interface. The R-CIGSSe device has a smaller recombination rate at the depletion region than the T-CIGSSe device, which is identified by *J–V* measurements (small ideality factor). These results reveal that the main limitation for achieving high efficiency of the R-CIGSSe device is the serious rear interface recombination and the back barrier Φ_B amounting to 499 meV. On the contrary, for the T-CIGSSe device, E_a is significantly improved to 1.116 eV, i.e., only 39 meV (equal to Φ_B), smaller than E_g (Figure 5b). Thus, the dominant recombination mechanism in the T-CIGSSe devices is bulk recombination rather than interface recombination.[6b] These results indicate that the dominant recombination path of the CIGSSe device can be changed from interface recombination to bulk recombination by utilizing Cu-In-TU-DMF for rear interface modification.

Combining the *J–V* and the *JV*(*T*) results, we derive the order of dominant recombination paths of these two CIGSSe devices: R-CIGSSe interface recombination (dominant recombination) > R-CIGSSe bulk recombination > T-CIGSSe bulk recombination (dominant recombination) > T-CIGSSe interface recombination and conclude that recombination can be significantly suppressed by the interface modification.

3. Conclusion

In summary, we have demonstrated that a Cu-In-TU-DMF layer for modifying the CIGSSe/ITO interface leads to a significant improvement in the device's performance. The T-CIGSSe device hence has a larger shunt resistance and a smaller reverse saturation current density than the R-CIGSSe device, confirming that the bulk recombination can be mitigated by interface modification. The open circuit voltage deficit of the T-CIGSSe device is significantly smaller than for R-CIGSSe, which can also be explained by the better absorber quality (smaller Urbach energy). The R-CIGSSe device has a smaller ideality factor, larger charge carrier density, and depletion width values. Yet, a significantly smaller value of barrier height is observed for the T-CIGSSe device, indicating that the rear interface modification is a simple and effective strategy to reduce interface recombination and improve the properties of submicron CIGSSe solar cells on TCO back contact. As a result, the champion efficiency of the rear interface modified CIGSSe solar cell achieves 7.9% with an open circuit voltage of 565.8 mV, a short circuit current density of 23.4 mA cm^{-2}, and a fill factor of 59.5%. The possible strategies to further improve the efficiency of semitransparent CIGSSe devices are 1) the introduction of NaCl pre-selenization treatment, and 2) the optimization of the Ga profile to increase the carrier diffusion length.

4. Experimental Section

ITO Back Contact Sputtering: Soda-lime glass (SLG) substrates (2.5 cm × 2.5 cm × 2 mm) were sequentially cleaned with acetone, isopropanol, and deionized water for 15 min each by sonication. Subsequently, the SLG substrates were dried by N_2 flow. A 400 nm ITO layer was deposited on the cleaned SLG substrates by DC-sputtering in a PRO Line PVD 75 (Kurt J. Lesker Company) thin-film deposition system.[2b,10] The ITO back contacts were subject to pre-annealing treatment at 500 °C for 10 min in an ambient atmosphere before spin-coating the precursor solution. Previous literature has proven that the pre-annealing treatment can improve the optical transparency and carrier mobility of ITO.[2c]

Formation of Precursor Solution: For the preparation of Cu-In-TU-DMF solution, first 46 mmol thiourea (TU, 99%, Alfa Aesar Company) was dissolved in 18 mL N, N-Dimethylformamide (DMF, ACS, 99.8%, Sigma–Aldrich) solvent to make a clear solution after 20 min stirring. Then, 7.77 mmol CuCl (99.8%, Sigma–Aldrich) was added to this solution and stirred until CuCl was completely dissolved. Finally, 8.45 mmol $InCl_3$ (99.8%, Sigma–Aldrich) was introduced, and a yellowish solution was obtained after overnight stirring. The solution was filtered by using a 0.45 µm polytetrafluoroethylene filter before spin-coating. For the Cu-In-Ga-TU-DMF solution, the 8.45 mmol $InCl_3$ was replaced by 2.53 mmol $GaCl_3$ and 5.92 mmol $InCl_3$ (Ga/(Ga+In) = 0.3).

Fabrication of CIGSSe Absorbers: The Cu-In-Ga-TU-DMF solution was spin-coated onto the ITO back contact with a speed of 1500 rpm for 60 s, and the wet film was immediately annealed on a hot plate at 350 °C for 2 min and moved to a ceramic plate for cooling down naturally. The spin-coating/annealing steps were repeated eight times to obtain a final absorber thickness of 730 nm. Subsequently, the as-obtained precursor films were selenized in a quartz tube furnace under a selenium atmosphere at 350 °C for 20 min and at 520 °C for 20 min before cooling down naturally. It should be noted that the quartz tube was evacuated and filled with argon three times before heating. This reference CIGSSe absorber is referred to as R-CIGSSe. For the CIGSSe absorber with an interface modification treatment (named T-CIGSSe), the first layer was replaced by the Cu-In-TU-DMF solution (without Ga). The other seven layers were spin-coated with Cu-In-Ga-TU-DMF solution.

Fabrication of CIGSSe Photovoltaic Devices: 10% KCN solution was utilized to etch the CIGSSe absorbers for 3 min to remove Cu_{2-x}(S,Se) and excessive Se. Then, an 80 nm thick CdS buffer was grown onto the CIGSSe absorbers by a chemical bath deposition process. An 80 nm i-ZnO and a 300 nm Al:ZnO layer were fabricated by RF-sputtering. Ni/Al top grids were deposited by thermal evaporation. The active area of each CIGSSe solar cell was 0.5 cm^2 defined by mechanical scribing. No antireflection coating layer was applied.

© 2023 The Authors. Advanced Materials Interfaces published by Wiley-VCH GmbH

21967350, 0, Downloaded from https://onlinelibrary.wiley.com/doi/10.1002/admi.202300566 by Universitaet Duisburg-Essen, Wiley Online Library on [07/11/2023]. See the Terms and Conditions (https://onlinelibrary.wiley.com/terms-and-conditions) on Wiley Online Library for rules of use; OA articles are governed by the applicable Creative Commons License

Characterization: The composition profiles of the CIGSSe absorbers were measured by glow discharge optical emission spectroscopy (GD-OES) using a Spectruma GDA 650 HR analyzer. For these measurements, the CdS buffer layer, the i-ZnO/AZO window layer, and the Ni/Al grid were removed from the solar cells used for electrical characterization. Morphological characterization was carried out using a JEOL JSM-7500F scanning electron microscope (SEM). The current density-voltage (*J–V*) curves were recorded under standard test conditions (AM1.5G; 100 mW cm^{-2}; 25 °C) by a WACOM sun-simulator containing both a Xenon and a Halogen lamp. The external quantum efficiency (EQE) was measured by a home-built system applying calibrated Si and Ge diodes as references. The capacitance-voltage (*C–V*) curves were taken under dark conditions with a BK PRECISION Model 895 operating at 100 kHz with a 5 mV testing signal. In addition, the temperature-dependent current density-voltage measurements were carried out in an enclosed liquid helium cryostat, with the temperature sensor mounted atop the sample.

Supporting Information

Supporting Information is available from the Wiley Online Library or from the author.

Acknowledgements

The authors thank Klaus Pärschke for the window layer and front contact deposition. Jeldrik Schulte, AG Winterer (UDE), is acknowledged for support with SEM measurements. The XRF and GDOES measurements were performed on an instrument funded by the Deutsche Forschungsgemeinschaft (DFG, German Research Foundation) – INST 20876/324-1 FUGG and are acknowledged as follows: "Gefördert durch die Deutsche Forschungsgemeinschaft (DFG) – Projektnummer INST 20876/324-1 FUGG". Y.G. especially acknowledges the financial support of the Chinese Scholarship Committee, and G.Y. the funding from the National Natural Science Foundation of China (NSFC, 51802240) and the funding support of the Fundamental Research Funds for the Central Universities (WUT183101002 and WUT193201003). The authors acknowledge support from the Open Access Publication Fund of the University of Duisburg-Essen.

Open access funding enabled and organized by Projekt DEAL.

Conflict of Interest

The authors declare no conflict of interest.

Data Availability Statement

The data that support the findings of this study are available from the corresponding author upon reasonable request.

Keywords

back interface modification, ITO back contact, pre-annealing treatment, solution process, submicron CIGSSe

Received: June 30, 2023
Revised: August 15, 2023
Published online:

[1] NREL Best Research-Cell Efficiency Chart, https://www.nrel.gov/pv/cell-efficiency.html (accessed: June 2023).

[2] a) J. Ramanujam, U. P. Singh, *Energy Environ. Sci.* **2017**, *10*, 1306; b) Y. Li, G. Yin, Y. Gao, T. Köhler, J. Lucaßen, M. Schmid, *Sol. Energy Mat. Sol. C* **2021**, *223*, 110969; c) L. Gouillart, A. Cattoni, J. Goffard, F. Donsanti, G. Patriarche, M. Jubault, N. Naghavi, S. Collin, *Thin Solid Films* **2019**, *672*, 1; d) T. Nakada, *Thin Solid Films* **2005**, *480–481*, 419; e) L. Gouillart, A. Cattoni, W. C. Chen, J. Goffard, L. Riekehr, J. Keller, M. Jubault, N. Naghavi, M. Edoff, S. Collin, *Prog. Photovolt.: Res. Appl.* **2021**, *29*, 212; f) A. Cho, I. Jeong, S. Song, D. Shin, S. Lee, K. Kim, J. H. Yun, J. S. Cho, J. H. Park, *Sol. RRL* **2021**, *5*, 2100485.

[3] a) V. Sousa, B. F. Gonçalves, Y. S. Rosen, J. Virtuoso, P. Anacleto, M. F. Cerqueira, E. Modin, P. Alpuim, O. I. Lebedev, S. Magdassi, S. Sadewasser, Y. V. Kolen'ko, *ACS Appl. Energy Mater.* **2020**, *3*, 3120; b) S. Suresh, A. R. Uhl, *Adv. Energy Mater.* **2021**, *11*, 2003743; c) T. Zhang, Y. Yang, D. Liu, S. C. Tse, W. Cao, Z. Feng, S. Chen, L. Qian, *Energy Environ. Sci.* **2016**, *9*, 3674; d) D. A. R. Barkhouse, O. Gunawan, T. Gokmen, T. K. Todorov, D. B. Mitzi, *Prog. Photovolt.: Res. Appl.* **2012**, *20*, 6; e) J. Jiang, S. Yu, Y. Gong, W. Yan, R. Zhang, S. Liu, W. Huang, H. Xin, *Sol. RRL* **2018**, *2*, 1800044; f) X. Lin, R. Klenk, L. Wang, T. Köhler, J. Albert, S. Fiechter, A. Ennaoui, M. C. Lux-Steiner, *Energy Environ. Sci.* **2016**, *9*, 2037.

[4] a) J. A. Clark, A. Murray, J. M. Lee, T. S. Autrey, A. D. Collord, H. W. Hillhouse, *J. Am. Chem. Soc.* **2019**, *141*, 298; b) J. Jiang, R. Giridharagopal, E. Jedlicka, K. Sun, S. Yu, S. Wu, Y. Gong, W. Yan, D. S. Ginger, M. A. Green, X. Hao, W. Huang, H. Xin, *Nano Energy* **2020**, *69*, 104438.

[5] Y. Kong, L. Huang, Z. Chi, X. Wu, J. Li, X. Xiao, *Acs Appl. Mater. Interface* **2020**, *12*, 52857.

[6] a) C. van Lare, G. Yin, A. Polman, M. Schmid, *ACS Nano* **2015**, *9*, 9603; b) G. Yin, M. W. Knight, M.-C. van Lare, M. M. Solà Garcia, A. Polman, M. Schmid, *Adv. Opt. Mater.* **2017**, *5*, 1600637; c) G. Yin, V. Brackmann, V. Hoffmann, M. Schmid, *Sol Energy Mat. Sol C* **2015**, *132*, 142; d) G. Yin, M. Song, M. Schmid, *Sol Energy Mat. Sol C* **2019**, *195*, 318.

[7] a) J. K. Larsen, H. Simchi, P. Xin, K. Kim, W. N. Shafarman, *Appl. Phys. Lett.* **2014**, *104*, 033901; b) M. J. Shin, S. Park, A. Lee, S. J. Park, A. Cho, K. Kim, S. K. Ahn, J. Hyung Park, J. Yoo, D. Shin, I. Jeong, J. H. Yun, J. Gwak, J.-S. Cho, *Appl. Surf. Sci.* **2021**, *535*, 147732; c) M. J. Shin, A. Lee, A. Cho, K. Kim, S. K. Ahn, J. H. Park, J. Yoo, J. H. Yun, J. Gwak, D. Shin, I. Jeong, J.-S. Cho, *Nano Energy* **2021**, *82*, 105729; d) A. Mavlonov, T. Nishimura, J. Chantana, Y. Kawano, T. Masuda, T. Minemoto, *Sol. Energy* **2020**, *211*, 1311.

[8] a) N. Barange, V. B. Chu, M. Nam, I.-H. Ahn, Y. D. Kim, I. K. Han, B. K. Min, D.-H. Ko, *Adv. Energy Mater.* **2016**, *6*, 1601114; b) J. Chantana, H. Arai, T. Minemoto, *J. Appl. Phys.* **2016**, *120*, 045302; c) Y.-S. Son, H. Yu, J.-K. Park, W. M. Kim, S.-Y. Ahn, W. Choi, D. Kim, J.-h. Jeong, *J. Phys. Chem. C* **2019**, *123*, 1635.

[9] S.-C. Yang, T.-Y. Lin, M. Ochoa, H. Lai, R. Kothandaraman, F. Fu, A. N. Tiwari, R. Carron, *Nat. Energy* **2022**, *8*, 40.

[10] Y. Gao, G. Yin, Y. Li, T. Köhler, J. Lucaßen, M. Schmid, *ACS Appl. Energy Mater.* **2022**, *5*, 12252.

[11] S. Ishizuka, J. Nishinaga, K. Beppu, T. Maeda, F. Aoyagi, T. Wada, A. Yamada, J. Chantana, T. Nishimura, T. Minemoto, M. M. Islam, T. Sakurai, N. Terada, *Phys. Chem. Chem. Phys.* **2022**, *24*, 1262.

[12] a) M. D. Heinemann, V. Efimova, R. Klenk, B. Hoepfner, M. Wollgarten, T. Unold, H.-W. Schock, C. A. Kaufmann, *Prog. Photovolt.: Res. Appl.* **2015**, *23*, 1228; b) J. Keller, L. Stolt, O. Donzel-Gargand, T. Kubart, M. Edoff, *Sol. RRL* **2022**, *6*, 2200401.

[13] A. Chirila, P. Reinhard, F. Pianezzi, P. Bloesch, A. R. Uhl, C. Fella, L. Kranz, D. Keller, C. Gretener, H. Hagendorfer, D. Jaeger, R. Erni, S. Nishiwaki, S. Buecheler, A. N. Tiwari, *Nat. Mater.* **2013**, *12*, 1107.

[14] J. Chantana, T. Nishimura, Y. Kawano, N. Suyama, A. Yamada, Y. Kimoto, T. Kato, H. Sugimoto, T. Minemoto, *Adv. Energy Mater.* **2019**, *9*, 1902869.

[15] S. S. Hegedus, W. N. Shafarman, *Prog. Photovolt.: Res. Appl.* **2004**, *12*, 155.

© 2023 The Authors. Advanced Materials Interfaces published by Wiley-VCH GmbH

21967350, 0, Downloaded from https://onlinelibrary.wiley.com/doi/10.1002/admi.202300566 by Universitaet Duisburg-Essen, Wiley Online Library on [07/11/2023]. See the Terms and Conditions (https://onlinelibrary.wiley.com/terms-and-conditions) on Wiley Online Library for rules of use; OA articles are governed by the applicable Creative Commons License

[16] a) J. Chantana, Y. Kawano, T. Nishimura, Y. Kimoto, T. Kato, H. Sugimoto, T. Minemoto, *ACS Appl. Energy Mater.* **2020**, *3*, 1292; b) J. Chantana, T. Nishimura, Y. Kawano, S. Teraji, T. Watanabe, T. Minemoto, *ACS Appl. Energy Mater.* **2019**, *2*, 7843.

[17] B. Duan, L. Guo, Q. Yu, J. Shi, H. Wu, Y. Luo, D. Li, S. Wu, Z. Zheng, Q. Meng, *J. Energy Chem* **2020**, *40*, 196.

[18] A. Villanueva-Tovar, T. Kodalle, C. A. Kaufmann, R. Schlatmann, R. Klenk, *Sol. RRL* **2020**, *4*, 1900560.

© 2023 The Authors. Advanced Materials Interfaces published by Wiley-VCH GmbH

21967350, 0, Downloaded from https://onlinelibrary.wiley.com/doi/10.1002/admi.202300566 by Universitaet Duisburg-Essen, Wiley Online Library on [07/11/2023]. See the Terms and Conditions (https://onlinelibrary.wiley.com/terms-and-conditions) on Wiley Online Library for rules of use; OA articles are governed by the applicable Creative Commons License